Earth Surf. Dynam. Discuss., 3, 417–458, 2015
www.earth-surf-dynam-discuss.net/3/417/2015/
doi:10.5194/esurfd-3-417-2015

Earth Surface Dynamics Discussions
Open Access

Tracing bedload transport in a high-elevation, formerly-glaciated mountain basin

A. Dell'Agnese[1], F. Brardinoni[2], M. Toro[3], L. Mao[4], M. Engel[1], and F. Comiti[1]

[1]Faculty of Science and Technology, Free University of Bolzano, Piazza Università 5, 39100 Bozen-Bolzano, Italy
[2]Department of Earth and Environmental Sciences, University of Milano-Bicocca, Piazza della Scienza 4, 20126 Milano, Italy
[3]Department of Civil and Environmental Engineering, University of Trento, Via Belenzani 12 I, 38122 Trento, Italy
[4]Department of Ecosystems and Environment, and Center of Applied Ecology & Sustainability (CAPES), Pontificia Universidad Católica de Chile, Avda. Libertador Bernardo O'Higgins 340, Santiago, Chile

Received: 22 April 2015 – Accepted: 27 April 2015 – Published: 21 May 2015

Correspondence to: A. Dell'Agnese (andrea.dellagnese@unibz.it)

Published by Copernicus Publications on behalf of the European Geosciences Union.

Abstract

In formerly glaciated mountain settings, Pleistocene glaciations are responsible for profound spatial reorganization of the landscape structure. By imposing local channel slope and the degree of hillslope-channel connectivity, glacial macro-forms can exert first-order controls on the downstream strength and continuity of the coarse sediment cascade. To estimate quantitatively these controls we trace bedload transport for three years along the Strimm Creek, Eastern Italian Alps. Specifically, we monitor the travel distance of 490 PIT-tagged particles (*b* axis: 23–229 mm; weight: 83–6525 g) at two contrasting sites: Upper Strimm Creek (US; 4 km^2), which flows through a fluvially-dominated hanging valley, and Lower Strimm Creek (LS; 7.5 km^2), located downstream, in a relict glacial trough where it experiences periodic colluvial sediment inputs from lateral tributaries. Tracer positioning within the streambed is periodically tracked in the field with a portable antenna in order to assess progressive travel distances, as well as the extent of the channel active layer, in relation to snowmelt and rainfall-driven peak flows. Cumulatively, tracers in US have travelled across distances (i.e., inner quartiles) shorter than 2 m, which correspond to over two orders of magnitude less than what observed in LS. These figures translate, after calculations of tracer inter-survey virtual velocities, in estimated bedload volumes equal to about 3 m^3 in US and 600 m^3 in LS, with most of the transport (75 % in US, and 93 % in LS) occurring during snowmelt. A similar contrast in bedload transport rates, even without considering the additional volumes of material mobilised by mass wasting process in LS, testifies the extent to which the glacial imprinting can still affect contemporary sediment transfer, and thus postglacial landscape evolution, in mountain drainage basins.

1 Introduction

The quantification of bedload transport rates and temporal variability in mountain streams is of primary importance in many applications in geomorphology, freshwater

ESURFD
3, 417–458, 2015

biology, and hydraulic engineering (Wohl, 2010), but, these still remain very difficult to predict (e.g., Comiti and Mao, 2012). Semi-empirical transport capacity equations proposed so far offer results heavily dependent on the experimental setup of the flumes or field conditions on specific study sites in which they were originally developed. When tested in mountain streams, these equations tend to overestimate the actual bedload transport rate by several orders of magnitude, especially when applied to ordinary flood events (e.g., Bathurst, 1987; Gomez and Church, 1989; Nakato, 1990; D'Agostino and Lenzi, 1999; Rickenmann, 2001; Habersack and Laronne, 2002; Martin, 2003; Nitsche et al., 2011; Green et al., 2015), mostly due to large macro-roughness providing extra energy dissipation and to the limited sediment supply conditions typical of stepped channels draining relatively small catchments (Montgomery and Buffington, 1997). Additionally, the actual dynamics of particle movement in such streams are possibly heavily influenced by the size, frequency, and spatial arrangement of morphological units.

A number of methods have been developed to investigate bedload transport over the last century. Among these, one of the oldest is represented by tracers, first used by Gilbert and Murphy (1914) in their pioneering work on the incipient motion of bed particles. During the last 50 years, several studies involving the use of tracers of different type have been conducted (e.g., Laronne and Carson, 1976; Hassan et al., 1991, 1992; Church and Hassan, 1992; Sear et al., 2000; Lenzi, 2004; Lamarre et al., 2005; Mao and Lenzi, 2007; Schneider et al., 2010; Liébault et al., 2012; Hassan et al., 2013). The way tracers work makes them ideal means for evaluating in-channel sediment connectivity over time (e.g., Bracken et al., 2014). In particular, they allow to gather quantitative information on thresholds for particle entrainment, transport distances and preferential resting sites, sediment sorting by particle size or shape, depth and width of the active layer (especially when complemented with scour chains), as well as on relative sediment transport rates.

The first tracers were simply painted stones (e.g., Takayama, 1965; Leopold et al., 1966), which provided precious insights on sediment mobility (e.g., Church and Hassan, 1992) but could not be recovered if buried. Substantial improvements on the detec-

ESURFD
3, 417–458, 2015

tion of buried tagged particles, hence on their recovery rate, were made by implanting small iron plates in natural clasts (surveys were conducted with a metal detector) using naturally magnetic tracers (Ergenzinger and Custer, 1983; Hassan and Ergenzinger, 2003). This technical solution allowed a more complete appraisal of the number of clasts moving from the surface to the subsurface (and vice-versa), which also meant gaining a better understanding of the active channel depth.

A more sophisticated system to trace particle movement was proposed by Schmidt and Ergenzinger (1992), who implanted active transponders into pebbles. These transponders emit a unique radio frequency identification code (RFID) detected and recorded by dedicated antennas. Even though active transponders have a wide detection range (order of meters, depending on their size), their use strongly relies on the duration of the internal battery. This is the main reason why passive integrated transponders (PIT) came into play. Originally developed to track fish passage in natural streams (e.g., Armstrong et al., 1996; Johnston et al., 2009), PIT were later used to monitor sediment movement (e.g., Nichols, 2004; Lamarre et al., 2005). The antennas used to detect PITs have a relatively short detection range (up to about 1 m, depending on PIT size), but PITs are small (down to 1 cm), cheap (approximately EUR 2,00 each) and do not require an internal battery.

Tracing the movements of single particles permits to calculate their virtual velocity, which, when analysed together with depth and width of the active channel layer, can lead to the assessment of bedload volumes transported by sequences of discrete transport events (e.g., Haschenburger and Church, 1998). Bedload tracing performed through portable RFID antennas has been applied successfully to inquire on bedload sediment dynamics in a number of fluvially-dominated settings, with recovery rates ranging from 60 to 100 % (e.g., Nichols, 2004; Lamarre et al., 2005; Lamarre and Roy, 2008; Schneider et al., 2010; Camenen et al., 2010; Liébault et al., 2012).

From a landscape evolution standpoint, monitoring bedload transport in mountain, formerly glaciated basins is key for quantifying contemporary rates of postglacial fluvial reworking in relation to landscape structure and degree of hillslope-channel ge-

ESURFD
3, 417–458, 2015

omorphic connectivity. In similar settings, the spatial organization of inherited glacial topography and glacigenic sedimentary covers – by modulating debris-flow sediment flux (Brardinoni et al., 2012), and by imposing sediment supply to stream channels (Brardinoni and Hassan, 2006; Brardinoni et al., 2009; Hoffman et al., 2012) – makes fluvial sediment dynamics at the basin scale complex and poorly understood. Although it is known that relict glacial macro-forms such has hanging valleys, valley steps, and troughs can control the spatial distribution of geomorphic process domains and channel-reach morphology (Brardinoni and Hassan, 2007; Weekes et al., 2012), a quantitative appraisal of the glacial conditioning on contemporary rates of bedload sediment transfer is still missing.

In this paper, we use 494 PIT-tagged clasts to evaluate bedload sediment transport in two strategic study sites within the Strimm Creek, a high-elevation, formerly glaciated basin of the Eastern Italian Alps. We aim to contrast the bedload transport regime of an upper site, located in a gentle hanging valley floor that is completely decoupled from colluvial sediment inputs, with the regime of a lower one located along a steep glacial trough and as such periodically affected by lateral mass-wasting sediment inputs. In particular, we track travel distances of tracers by means of a portable RFID antenna from August 2011 to July 2014, and quantify bedload transport over a three-year time period. After characterizing the downstream variability in channel boundary conditions, we analyse tracer travel distances and virtual velocities in relation to peak discharge and tracer weight. Finally, we estimate transported bedload volumes in the two study sites and put forward postglacial patterns of sediment transfer at the basin scale.

2 Study area

The Strimm Creek (drainage area 8.5 km^2) is a rugged, formerly glaciated basin located in the upper Vinschgau/Venosta Valley, corresponding to the upper portion of the Etsch/Adige River, Eastern Italian Alps (Fig. 1). Elevation ranges from 1394 m, at the basin outlet, to 3197 m a.s.l. The basin has a peculiar elongated shape, with

ESURFD
3, 417–458, 2015

a roughly homogeneous width of about 1 km. Most of the upper portion of the Strimm basin is underlain by paragneiss and schist with abundant metapegmatites of the Mazia unit (Habler et al., 2009), except for the distal-most part, in which paragneiss and orthogneiss of the Öztal unit outcrops (C. Morelli, personal communication, 2015, based on unpublished data of the CARG project, Provincia Autonoma di Bolzano). The annual average precipitation in the Etsch/Adige valley is quite low, being around 480 mm at the valley floor (Laas/Lasa weather station, 863 m a.s.l., period 1989–2012), with maxima in July and August. Precipitations increase in the lower Strimm basin (662 mm, at the Strimmhof station, 1754 m a.s.l., period 1993–2012 – R1 in Fig. 1), and even if long-term series for the upper part of the basin are not yet available, an estimated value of about 800–900 mm is probable. At the Strimmhof station, the max precipitation over a 24 h period recorded between 1993 and 2012 amounts to 72 mm. Since July 2011, a non-heated rain gauge (R2, Fig. 1) powered by a solar panel was installed at 2560 m a.s.l. to monitor summer (May to October) rainstorms triggering debris flows in the adjacent Gadria Creek (Comiti et al., 2014). Snow cover in the intermediate and upper parts of the Strimm basin usually lasts from November to early June, but largely varies depending on site aspect.

Currently active geomorphic processes include periglacial, colluvial, and fluvial transport. Periglacial activity is prevalent on the talus slopes of the upper Strimm basin, as testified by the presence of intact rock glaciers on east- and north-facing slopes above 2600 m a.s.l. Perennial fluvial transport regime characterizes the lower half of the hanging valley floor (slope range: 1–8 %) downstream of the large hummocky moraine, and down to the basin outlet (Fig. 1). This upper part of the study stream is disconnected from colluvial sediment inputs (Fig. 2a and b) except at one location, where small debris flows deliver material eroded from a till-mantled valley side (Fig. 1). In the middle part of the basin (valley slope range: 10–25 %), downstream of the rocky valley step that marks the transition between the hanging valley and the steep glacial trough, debris slides and channelized debris flows convey colluvial material from colluvial tributaries to the main channel. In the distal part, downstream of WS1 (Fig. 1), Strimm Creek devi-

ESURFD
3, 417–458, 2015

ates towards south-east flowing in a structurally-controlled, V-notched valley step with no lateral tributary (Fig. 2d). Here open-slope debris slides and bank failures deliver material directly to the channel. This is the steepest part of Lower Strimm, with slope ranging between 12 and 42 %.

The bedload monitoring sites are located within the hanging valley floor (Upper Strimm) and downstream of the rocky valley step (Lower Strimm). Upper Strimm, hereafter termed US (average slope = 3 %), is characterized by plane-bed and step-pool channel morphologies (Fig. 2a and b). Lower Strimm, hereafter termed LS (average slope = 10 %), is dominated by boulder-cascades and step-pools (Fig. 2c and d). The former is located at about 2550 m a.s.l., above the tree line, the latter sits at about 1850 m and flows amidst coniferous forest dominated by European larch (*Larix decidua* (M.)) and Norway spruce (*Picea abies* (L.)).

3 Methods

Water stage monitoring is conducted by means of two stand-alone, battery-powered pressure transducers installed at the downstream end of the hanging valley (WS2, Fig. 1, elevation 2430 m a.s.l., drainage area 4 km^2) and near the basin outlet (WS1, Fig. 1, elevation 1830 m a.s.l., drainage area 7.5 km^2). Both stations record water level every 10 min, year-round. Relevant flow rating curves are derived from salt dilution (slug injection) discharge measurements. Owing to frequent cross-sectional changes at WS1, we use this station only for confirming the occurrence of flood events, whereas the quantitative analysis on particle displacement at US and LS is based on WS2 flow data, where the cross-section remained stable over the entire period. Based on 10 concurrent discharge measurements, flows in WS1 result on average 60 % higher than at WS2 during snowmelt, and about 100 % higher during summer low flows. Errors associated with these estimates will be later accounted for in the analysis of Lower Strimm.

ESURFD
3, 417–458, 2015

Before preparing the PIT-tagged stones for bedload tracing, we characterized the surface grain size distribution at US and LS. This was performed through 34 grid-by-number pebble count samples (grid spacing 0.3 at US, 0.5 m at LS; Bunte and Abt, 2001). Surface grain size curves were then derived for both sites by integrating all the 34 samples (Fig. 3a). In the upper study area, sediments range from 4 to 512 mm, with a SD of 2.1. The lower study area is comparatively coarser, with *b* axis varying from 5.6 to 1024 mm, and a much more heterogeneous distribution (SD 3.37).

To investigate bed mobility, particle travel distances, and bedload volumes in the two contrasting study sites (US and LS) of Strimm Creek we used painted, PIT-tagged clasts. PITs (23.1 mm long and 3.85 mm in diameter) manufactured by Texas Instruments were implanted within drilled clasts and glued into the holes with epoxy resin. PIT-tagged clasts were then released on the streambed as transverse ribs along the study sites with a downstream spacing of 5 m in US and 3 m in LS. Each rib at US consisted of 3 to 4 clasts, one of which always located on the thalweg, and the other two near the banks. At LS, ribs consisted of 4 clasts, two of which were always deployed in the centre of the channel. In order to assess the variability of active channel width during higher flows, additional clasts were added to a given transverse rib in correspondence of bars or other lateral deposits.

In the US study site we released a total of 259 painted PITs (Table 1) (*b* axis ranging from 23 to 155 mm; weight from 89 to 1482 g) in three sequential sets: on 31 August 2011 (80 PITs), 28 September 2011 (79 PITs), and 14 June 2012 (100 PITs). At LS, we released a total of 231 painted PITs (*b* axis ranging from 35 to 229 mm; weight from 83 to 6525 g) (Table 1). Initially, we released 101 painted PITs on 25 July 2011 and 69 more on 29 August 2011. On 4 July 2013, 61 additional clasts (*b* axis ranging from 48 to 132 mm) were released at the same site as a consequence of the intense snowmelt recorded in summer 2013, during which 120 tracers of the initial ones exited the study area travelling to the steep and inaccessible downstream-most reach. The grain size distributions of the tracer particles released in the two study sites mimic

ESURFD
3, 417–458, 2015

the coarser nature of LS in comparison to US (Fig. 3b), with the minimum tracer size dictated by the size of the PIT tags.

A detailed topographic survey at US was performed during 2011–2012 by means of a monopod laser range finder (MDL LaserAce 300), for a total surveyed length of 1093 m. The survey featured a minimum density of 3 points m^{-1} along the thalweg, with additional points collected on the active streambed to define macro-forms. The topographic survey of the LS segment (total length 1514 m) was performed earlier, during October 2010 and May 2011, with a Leica T1000 total station. This survey featured a minimum point density of 2 points m^{-1} along the thalweg, with several additional points surveyed to better define the step-pool morphology and avoid data loss due to the smoothing of the model. Concurrently, we surveyed a total of 120 channel cross-sections at intervals of 20 and 25 m respectively in US and LS (Fig. 1). The digital delineation of the main channel, the derivation of the contributing area (A), and the characterization of relevant channel boundary conditions (i.e., local channel slope (S), and indices of total (Ω) and unit (ω) – stream power) was conducted via integration of the foregoing field-based data with aerial photo interpretation and an airborne LiDAR-derived 1 m DEM acquired in 2011 (Fig. 1). Indices of total stream power ($\Omega = AS$) and specific stream power ($\omega = AS/w_{bf}$) were obtained by replacing water discharge with contributing area (e.g., Brummer and Montgomery, 2003).

Bedload tracing was conducted by means of portable RFID antennas (one manufactured by AQUARTIS, one by Oregon RFID) from spring to autumn depending on the occurrence of flow events (e.g., snowmelt, rainfall-induced, and a combination of the two; Fig. 4). The relative position of each clast was measured from a series of georeferenced control points along the topographic net created during the 2010–2012 surveys, so that, after each survey, it was possible to derive the absolute position of the clasts. The relative displacement of each tracer was then calculated by measuring along the thalweg the distance from their actual position to the position identified during the previous survey.

ESURFD
3, 417–458, 2015

Even though we have measured the three axes of each tracer stone, we will show the results of travel distance in relation to tracer weight only. This is because statistical relations within site and across grain-size categories exhibit much higher scatter (likely due to their highly variable shapes) and because assessing the effect of particle shape on sediment transport is beyond the scope of this work. For reference, we report the relation between tracer weight and tracer b axis ($R^2 = 0.67$; Fig. 3c). In our analysis, the tagged particles were grouped into eight weight categories, (W1 to W8, Table 2). At US, the uncertainty associated with the positioning of single tracers due to instrumental errors, was estimated to be 0.2 m. Here the painted PITs were consistently visible during fieldwork thanks to the low turbulence and rare burial conditions. By contrast, in LS, where often clasts were buried or difficult to locate with greater accuracy due to the more turbulent nature of the flow and the rougher bed texture, instrumental uncertainty was estimated to be up to 0.5 m. All estimated movements lower than these tolerance thresholds were discarded from the analysis.

We used the flow competence method for assessing sediment mobility (e.g., Andrews, 1983), with the minimum discharge able to entrain clasts of each weight class identified based on the field surveys. The discharge value related to the motion threshold was defined as:

$$Q_t = \min\left\{\max\left(Q_i\right); \min\left(\overline{Q}_i\right)\right\} \quad (1)$$

where Q_i are the discharge values for which clasts from the ith weight class remained immobile and $\overline{Q}_i$ the values for which clasts of the ith weight class moved.

Virtual velocities were quantified considering the displacement length and the duration of over-threshold flows between two subsequent surveys, and were used to estimate the total sediment transported during the survey period. This approach was preferred over a shear stress-based one due to the extremely rough geometry of the channel, which would have made the estimation of the water depth at different sections subject to greater uncertainties (Comiti and Mao, 2012). Following Liébault and Laronne (2008) among others, the volumetric bedload transport volume (G [m^3]) was

ESURFD
3, 417–458, 2015

then assessed as:

$$G = d_s w_s \overline{v} (1 - p) \quad (2)$$

where w_s [m] is the mean width of the active channel bed, d_s [m] the depth of the active layer of sediments, $\overline{v}$ the mean virtual velocity of the transported clasts, and p the fractional porosity of channel sediment (here assumed to be equal to 0.3). The volumetric transport rates were then multiplied by the integral transport time (i.e., total time for which the threshold discharge value was reached or trespassed) to derive volumes moved during each intra-survey period.

The depth of the active layer was estimated to be equal to the maximum diameter (*b* axis) of the locally displaced particles (Table 1 and Fig. 3). This approximation, which is based on digging tests conducted on a subset of buried tracer stones, is in agreement with a recent study conducted in high-gradient, boulder-bed streams in the Alps showing that during ordinary events the thickness of the active layer ranges between 0.01 and 0.22 m (Schneider et al., 2014). Furthermore, Houbrechts et al. (2012) have shown that the thickness of the active layer in mountain streams is typically lower than the D_{50}.

Because the main channel is well confined in both study sites, and since the distribution of tracer travel distances across single transverse ribs did not show any cross-sectional variability (i.e., tracers located near the banks or in the centre of the streambed displayed the same degree of mobility), we approximated active channel width with the local bankfull width in US and LS, which is 3.5 and 4 m, respectively (Fig. 5).

ESURFD
3, 417–458, 2015

4 Results

4.1 Downstream variability in channel characteristics

Inspection of characteristic percentiles (i.e., D_{50}, D_{84}, and D_{90}) of surface grain-size distribution as a function of downstream distance (Fig. 5a), while confirming that surface bed texture is considerably coarser in LS than in US, indicates consistent patterns of downstream fining within the two sites. These patterns are interrupted by the rocky valley step that separates the decoupled hanging valley from the glacial trough, downstream of which sediment caliber resets at markedly higher values, as lateral sediment supply from debris flow-dominated tributaries feeds lower Strimm Creek. Downstream fining, in terms of D_{50}, appears to be more efficient in LS than in US: i.e. D_{50} declines from 120 to 50 mm in LS, and from 83 to 52 mm in US, which correspond to average fining rates of 40.5 mm km^{-1} in LS and 28.4 mm km^{-1} in US. In comparison, the coarser fractions exhibit a much higher scatter in the distal portion of LS, where downstream fining is less obvious.

Bankfull channel width exhibits a complex behavior. At the headwaters we observe strong downstream narrowing followed by some widening in the distal part of US (Fig. 5b). Downstream narrowing is due to the morphological transition from ephemeral, poorly-defined wide and shallow bed (Fig. 2b), where channelized runoff is quickly increased by subsurface flows moving away from the hummocky moraine (i.e., the lake area in Fig. 1), to a perennial channel characterized by a defined alluvial bed and higher channel banks (Fig. 2c). Downstream widening continues gradually along LS (Fig. 5b). Both indices of total and unit stream power increase fast throughout US, with a maximum in the US distal-most cross-sections, and stay nearly constant along LS, with locally high fluctuations especially in terms of total stream power (Fig. 5b).

ESURFD
3, 417–458, 2015

4.2 Particle displacement in Upper Strimm

The first survey, performed on 28 September 2011 (intra-survey maximum water discharge $Q_{max} = 0.36\,m^3\,s^{-1}$) showed that 77 out of the initial 80 deployed clasts remained immobile, and that the three clasts moved for a maximum distance of 1.2 m. No clast from classes W1, W4 or W6 moved. The survey performed on 14 June 2012 ($Q_{max} = 0.66\,m^3\,s^{-1}$), immediately after the end of the snowmelt period, showed that 44 out of 159 clasts had moved, with displacements occurring in all weight classes, and a maximum travel distance of 4.5 m. By 3 July 2012 (intra-survey maximum discharge of $0.55\,m^3\,s^{-1}$) only 12 clasts out of 259 experienced mobility (maximum displacement = 3.4 m), and no movement recorded for clasts belonging to classes W3 to W6. On 11 September 2012 ($Q_{max} = 0.33\,m^3\,s^{-1}$), the survey showed that 44 clasts (out of 255 recovered) moved over a maximum distance of 3.9 m, with no movement in class W6. By 4 October 2012 ($Q_{max} = 0.32\,m^3\,s^{-1}$) only 11 clasts out of the 253 recovered were entrained, with no motion in classes W4 to W6, and a maximum travel distance of 1.6 m for one clast in class W2.

As a consequence of a deep snowpack present on the ground until late spring 2013, the snowmelt season of this year featured high discharges sustained for a long period (cf. Fig. 4). Accordingly, on 27 June 2013 ($Q_{max} = 1.13\,m^3\,s^{-1}$) we recorded the motion of 123 clasts (out of 242 recovered) for up to 35 m (one clast in class W1), which represents the maximum distance recorded in US during the entire study period. The last 2013 survey was conducted on 1 October ($Q_{max} = 0.72\,m^3\,s^{-1}$), when 91 clasts (out of 239 recovered) belonging to all weight classes moved (max displacement of 12 m for a particle in W2). The final survey was associated with the snowmelt of 2014. On 13 June 2014 ($Q_{max} = 0.95\,m^3\,s^{-1}$) we recorded 95 displaced clasts (out of 234 recovered), with a maximum distance of 23.8 m.

A comprehensive view of the eight field surveys in US can be obtained by plotting histograms of clasts displaced stratified by five travel distance categories and by tracer weight classes (Fig. 6, left hand panels; Table S1 in the Supplement). This representa-

ESURFD
3, 417–458, 2015

tion shows how larger proportions of tracers are systematically displaced by snowmelt flows compared to rainfall-related ones. This is exemplified by surveys conducted in June, during which some movement was recorded in all weight classes (W1 to W6) (Fig. 6c, n, and r).

For each intra-survey value of Q_{max}, weight classes were plotted against the maximum travel distance during that period (Fig. 7a). Selected plots suggest that particle entrainment in US appears to be size-selective (sensu Parker et al., 1982) for the coarser classes as these are transported across shorter distances by each explored discharge. Boxplots of tracer travel distance (d) across weight classes (W) (Fig. 7b) show that median values decrease progressively for heavier particles, passing from 0.90 m (W1) to 0.50 m (W6), class W5 being the only exception with the highest median (1.0 m). Interestingly, the one-order magnitude decline of the maximum travel distance (i.e., d_{max} decreases from 35 m (W1) to 3.9 m (W6)) indicates that increasingly heavier clasts are bound to travel less and less, in agreement with what observed in Fig. 7a.

4.3 Particle displacement in Lower Strimm

The first survey, completed on 27 September 2011 ($Q_{max} = 0.58\,m^3\,s^{-1}$), showed that only 24 PITs moved, with maximum travel distances of 33.9 m (class W2), 30.6 m (W5), and greater than 10 m (W3, W6, and W7), and no motion recorded in W1 and W4. The survey conducted on 18 May 2012 ($Q_{max} = 0.53\,m^3\,s^{-1}$) showed that 84 out of 170 clasts moved, with maximum travel distances of 6.1 m (W4) and 17.2 m (W5). Travel distances increased substantially due to the peak snowmelt discharge ($Q_{max} = 1.05\,m^3\,s^{-1}$), so that by 28 June 2012 only 23 out of 170 clasts remained immobile, while the others moved over greater distances (one order of magnitude) than previously observed. Specifically, 26 clasts moved between 300 and 500 m, and 11 over 500 m, with a peak travel distance of 937 m (W8 peak travel distance = 238 m). During the intra-survey period ending on 21 August 2012, peak discharge lowered considerably ($Q_{max} = 0.65\,m^3\,s^{-1}$), returning to values comparable to those recorded in May. As a consequence, travel distances mimicked those observed in May, with 62

ESURFD
3, 417–458, 2015

particles (out of 165 recovered) displaced. Maximum travel distance was highest in W3 (21.7 m), lowest in W8 (1.7 m), and only 9 clasts (in classes W1 and W4) moved further than 10 m. On 25 October 2012, after a period characterized by slightly lower peak discharge ($Q_{max} = 0.51\,m^3\,s^{-1}$), we recorded results in line with what observed in the previous survey: with 60 clasts (out of 164 recovered) displaced. Among these, 58 travelled < 10 m, and only 2 over greater distances.

As also recorded in US, 2013 was characterized by a very late snowmelt, with snow cover in the upper part of the basin lasting until the end of May. On 21 May 2013 ($Q_{max} = 0.38\,m^3\,s^{-1}$) we recorded that 120 clast (out of 164 recovered) did not move, 42 moved over relatively short distances (< 10 m), and only 2 moved further away (< 30 m). By 2 July 2013, after the high snowmelt flows ($Q_{max} = 1.81\,m^3\,s^{-1}$) had ceased we observed the displacement of 158 clasts (out of 164 recovered). In particular, 105 tracers travelled for more than 500 m, 11 of which between 300 and 500 m, with a peak displacement of 927 m. Displacements associated with summer storms were assessed on 2 October 2013 ($Q_{max} = 1.01\,m^3\,s^{-1}$). By this date, 78 clasts (out of 130 recovered) had moved, mostly across relatively short distances (60 clasts < 10 m; 11 between 10 and 30 m, and only one > 30 m), but with some exceptionally high peaks (959 and 918 m for single clasts belonging respectively to W1 and W2). All weight classes moved, with the heaviest presenting peak displacements of 7.7 m (W7) and 10.0 m (W8). In the final post-snowmelt survey, conducted on 16 July 2014 ($Q_{max} = 1.51\,m^3\,s^{-1}$), we observed displacements in all weight classes, with a combined mobilization of 82 tracers (out of 127 recovered). In particular, we measured a peak travel distance of 958 m (W5), we recorded that 10 clasts had travelled between 300 and 500 m, and 8 clasts further away.

Summary information on clast movements for each weight class and stratified by travel distance (Fig. 6, right hand panels; Table S2) confirm also for LS the seasonal character observed in US, with largest displacements associated with snowmelt hydrographs. In particular, in the three surveys conducted in June we recorded tracer displacement > 50 m in all weight categories (W1 to W8) (Fig. 6f, o, and s), whereas

ESURFD
3, 417–458, 2015

similar magnitude length steps associated with rainfall-induced events were observed in some weight classes in 2013 only (Fig. 6q).

Overall, maximum travel distances at LS appear to be less sensitive to Q_{max} (Fig. 8a) compared to what observed in US, as they range over the same order of magnitude for peak flows $> 0.65\,m^3\,s^{-1}$, thus suggesting a tendency to equimobility conditions above this threshold. Boxplots of clast displacement (d) across weight classes (W) during the study period (Fig. 8b) show comparable ranges of variability, both in terms of inner (25–75 %) and outer (< 25 and > 75 %) quartiles. The latter shrink progressively for classes W7 and W8. Median displacement is constrained between 6.2 and 11.1 m, class W2 being the only exception with a value one order of magnitude larger (d_{med} = 187.2 m). Overall, these observations corroborate the hypothesis that near equimobility conditions in LS are established within the explored grain size classes.

4.4 Particle virtual velocities and estimated bedload volumes

The flow competence method (Eq. 1) allowed to identify different thresholds for sediment motion for the two study sites. At US, discharges $> 0.32\,m^3\,s^{-1}$ were able to mobilize clasts from all weight classes (W1 to W6). This figure is slightly lower than what estimated at LS, where entrainment across all classes (W1 to W8) occurred for flows $> 0.38\,m^3\,s^{-1}$. Given the uncertainty associated with water discharge at LS, we consider the two values not significantly different.

Thresholds for sediment motion in US and LS were used to estimate the integral duration of transport for each tracer class. These values were then used to calculate tracer virtual velocity for each intra-survey period, defined as the ratio between the mean displacement length and the integral transport time. In US, boxplots of virtual velocities as a function of intra-survey peak flow (Fig. 9a) identify a high-velocity envelope ($0.1 < \overline{v} < 10\,cm\,s^{-1}$) for low flows ($Q_{max} < 0.36\,m^3\,s^{-1}$), and a low-velocity one ($0.001 < \overline{v} < 0.1\,cm\,s^{-1}$) for higher flows. At first sight this behavior appears counterintuitive. However, when stratifying peak flows in snowmelt, rainstorm-driven and mixed regimes (cf. Fig. 4), and recalling that clast virtual velocity includes both travelling and

ESURFD
3, 417–458, 2015

resting periods, it becomes apparent that the high velocity envelope is associated with short-duration (i.e., hours) summer storms. In these periods, characterized by lower peak discharges, a greater precision on the identification of the threshold discharges is possible, so that the integral time calculated for virtual velocities tends to approach the real time of the particle movement, resulting in virtual velocities that are more representative of the tracer's actual velocity. Conversely, the low-velocity envelope is the expression of long-duration, sustained snowmelt flows (i.e., months) wherein potentially long resting periods are present as well. The fact that for purely snowmelt inter-survey periods median virtual velocity increases gradually with peak flow (i.e., $Q_{max} = 0.72\,m^3\,s^{-1}$ is associated with a mixed hydrologic forcing including part of the exceptionally long 2013 snowmelt runoff and summer storms, cf. Fig. 4) seems to corroborate this interpretation.

In LS we observe a more complex pattern in that rainfall- and snowmelt-dominated inter-survey periods cannot be discriminated in terms of virtual velocities (Fig. 9b), possibly as a consequence of integrating a larger drainage area (i.e., for convective summer storms) and lower elevations (i.e., for snowmelt events). Similarly to what observed in US, virtual velocities during snowmelt flows increase progressively with peak flow rate. Mixed snowmelt-rainfall events ($Q_{max} = 0.53$ and $0.65\,m^3\,s^{-1}$) lie consistently below rainstorm-related velocities. The highest median virtual velocity is associated with an early secondary snowmelt peak ($Q_{max} = 0.38\,m^3\,s^{-1}$), characterized by no rainfall inputs (cf. Fig. 4), occurring before the main snowmelt runoff in spring 2011.

In order to gain further insights on the effects that hydro-meteorological forcing can exert on bedload sediment transport, virtual velocities of single tracers were plotted – for selected intra-survey periods – as a function of their weight (Fig. 10). In particular, we compare the effects of the same snowmelt (i.e., spring–summer 2013) and rainfall season (i.e., summer–fall 2012) on tracer virtual velocity in US and LS. Results show that rainfall-induced peak flows have almost identical effects in the two study sites by imparting virtual velocities clustered between 0.1 and $3\,cm\,s^{-1}$. Interestingly, we observe a direct weak correlation between tracer weight and virtual velocity. By contrast,

ESURFD
3, 417–458, 2015

snowmelt discharges appear to make the main difference between US and LS, with the latter characterized by a tight cluster of virtual velocities centred around 1 cm min^{-1} (Fig. 10a), about two orders of magnitude higher than the centroid observed in US (Fig. 10b). In both instances, mixed rainfall-snowmelt inter-survey periods generate virtual velocities clustered within the lowest range of magnitudes.

Following the approach based on tracer virtual velocities and the field-based evaluation of the active layer width and depth (see Sect. 3), we estimated bedload transport volumes in US (Table 3) and LS (Table 4) across the three-year study period (Fig. 11). Cumulatively, in the monitored portions of US and LS bedload volumes amounts to respectively 3.3 and 590 m^3 (Fig. 11b), which correspond to approximately 2.9 and 511 tonnes per year. In agreement with what noted above in terms of virtual velocity clustering for different hydro-meteorological forcing (cf. boxplots in Fig. 9a and b), this two-order of magnitude difference is mainly controlled by the higher efficiency of snowmelt-driven bedload transport in LS (Fig. 11a), and to a lesser extent by rainfall and mixed events. Specifically, snowmelt-related transport accounted for 75 % in US and 93 % in LS of the total bedload flux.

5 Discussion

The structure of the Strimm basin is the result of Pleistocene glacial activity that reshaped the complex, tectonically-controlled landscape structures typical of the Austroalpine metamorphic domain. As a result, the spatial organization of relict glacial macro-forms bears some structurally-controlled inheritance. For example, the locations of the hanging valley and the rocky valley step are not associated with a relict ice flow confluence, nor with the development of a glacial overdeepening. This landscape structure, by imposing local channel slope and the degree of hillslope-channel connectivity, has affected and still controls the pace of postglacial landscape evolution in different portions of the Strimm Creek. In particular, Upper Strimm Creek flows through a relatively gentle channel bed in decoupled conditions, characterized by indices of stream

ESURFD
3, 417–458, 2015

power that are about one order of magnitude smaller than in the steeper and strongly coupled Lower Strimm Creek (Cavalli et al., 2013). Contrasting hillslope-channel coupling conditions in the two study sites have generated strikingly different channel types on the opposite sides of the rocky valley step, including purely-alluvial channel reaches in US (D_{84} = 119 mm; D_{90} = 148 mm) and much rougher, semi-alluvial ones (e.g., Halwas and Church, 2002) in LS (D_{84} = 281 mm; D_{90} = 368 mm).

By means of a three-year bedload tracing effort, we show that the contrasting channel boundary conditions at US and LS respond in markedly different ways to the snowmelt-dominated hydrologic regime of the study basin, which is characterized by low annual and summer precipitation. Here, sediment transporting flows occur during snowmelt (generally between mid May and late June), and to a lesser extent during summer convective storms. Cyclonic fronts from late October through November typically bring snow to the upper basin, thus autumn floods do not occur. In both study sites, we observe that most of the bedload material is mobilized during the snowmelt period, but with tracer maximum travel distances in LS that are one to two orders of magnitude larger than in US.

In US, bedload transport appears to function in a highly weight-selective fashion, with tracers heavier than 1 kg being mobilized sporadically and for distances < 10 m. By contrast, in LS, characterized by roughly 60 % higher peak discharges, all the monitored clast categories tend to move across comparable orders of distances, with snowmelt events able to transport heavier particles (> 5 kg) for distances > 50 m. These quantitative observations translate, for a given snowmelt event, in virtual velocities that in LS are about two orders of magnitude higher than in US, whereas rainfall-driven transport events are associated with more comparable figures in the two study sites. In turn, such a disparity in tracer virtual velocities results in amplified differences in terms of estimated bedload transport volumes, so that in the entire study period about 200 $m^3\,year^{-1}$ were transported in LS, as opposed to only a little more than 1 m^3 in US. Of these volumes, snowmelt flows are responsible for respectively 93 and 75 % of the total in LS and US.

ESURFD
3, 417–458, 2015

In order to fully estimate contemporary rates of sediment transfer in the Strimm Creek basin, it is important to consider the "ordinary" bedload transport volumes estimated during the study period in conjunction with high-magnitude events able to reorganize the streambed, in particular with the sediment volume transported during the large complex event occurred on 12 July 2010 (Fig. 12). On that occasion, about 22 mm of rain (measured approximately within twenty minutes at gauge R1) triggered a debris-flow event that reached the retention dam at the basin outlet (Fig. 1). The post-event survey, conducted by some of the authors together with technicians of the local river basin agency, identified complex spatial dynamics. While the main channel up in the US site showed no evidence of significant bedload transport or bed changes, most of the western colluvial tributaries located just downstream of the valley step were affected by debris flows, which fed the main channel with large sediment supply (Fig. 12). Peak discharges up to 40–50 $m^3 s^{-1}$ were estimated at the LS site, where the flow was probably a debris flood (Hungr, 2005), based on direct morphological and sedimentological field evidences. However, only moderate incision was apparent at the LS site after the event. More severe was the bed incision which took place in the steep, lower-most reach of Strimm Creek, where several landslides were triggered by slope undercutting and increase the sediment concentration of the flow, probably up to debris flow levels.

The topographic survey conducted at the retention basin (Fig. 1) determined that the 2010 event transported about 15 000 m^3 of debris. This event represents the largest recorded in the provincial geo-hazard database for the study basin, and locals claim that an event of similar magnitude occurred only back in the 1930s. Remarkably, this volume of material, which was all recruited downstream of the rocky valley step, corresponds to an equivalent of about 20–25 years of "ordinary" bedload transport, making Strimm Creek, in the present climatic conditions, a bedload-dominated system.

ESURFD
3, 417–458, 2015

6 Conclusions

By tracking bedload particle movement simultaneously at two sites, we quantify an increase in bedload transport greater than two orders of magnitude moving from the hanging valley in Upper Strimm Creek, through the disconnecting rocky valley step, and down to the reaches within the glacial trough in Lower Strimm Creek. We show that geomorphic conditions of hillslope-channel decoupling correspond to comparatively lower rates of downstream sediment fining (i.e., 28.4 mm km^{-1}) and to low, within-channel sediment connectivity (i.e., low bedload transport) along the monitored reaches in US. Conversely, strongly-coupled conditions ensure strikingly increased efficiency in sediment evacuation and stronger downstream sediment fining (i.e., 40.5 mm km^{-1}) in LS reaches.

Notwithstanding the limited length of record and the uncertainty associated with the calculation of bedload transport volumes through the virtual velocity approach, the combination of high-magnitude, low-frequency floods/debris flows with estimates of bedload transport events presented here, in consideration of the contrasting rates of landscape down-wasting in the upper and lower portions of the investigated basin, points to a postglacial evolution of a typical alpine mountain basin like Strimm Creek in which glacial topographic signatures (e.g., Brardinoni and Hassan, 2006) will likely amplify rather than reduce. In particular, the low rate of bedload material supplied to the bedrock channel cutting through the valley step will keep the "tool effect" to low levels of efficiency, whereas the degree of channelized landscape dissection in LS will continue to grow comparatively faster thanks to the combined work of bedload and mass wasting processes.

The Supplement related to this article is available online at doi:10.5194/-15-417-2015-supplement.

ESURFD
3, 417–458, 2015

Acknowledgements. This project was made possible thanks to the funds granted by the projects “Monitor II” (EU Interreg South-East Europe), “GESTO” (granted by the Autonomous Province of Bolzano) and “SEDALP” (EU Alpine Space programme). Gianluca Abram, Giulia Bonfanti, Alex Boninsegna, Enrico Buzzi, Marco Chiolo, Giacomo Falsitta, Raffaele Foffa, Ana Lucìa, Alberto Maggioni, Enrico Marchese, and Emilio Perina are kindly acknowledged for their precious field assistance.

References

Andrews, E. D.: Entrainment of gravel from naturally sorted riverbed material, Geol. Soc. Am. Bull., 94, 1225–1231, 1983.

Armstrong, J. D., Braithwaite, V. A., and Rycroft, P.: A flat-bed passive integrated transponder antenna array for monitoring behaviour of Atlantic salmon parr and other fish, J. Fish Biol., 48, 539–541, 1996.

Bathurst, J. C.: Measuring and modelling bedload transport in channels with coarse bed materials, in: River Channels – Environment and Process, edited by: Richards, K., Blackwell, Oxford, 272–294, 1987.

Buffington, J. M. and Montgomery, D. R.: A systematic analysis of eight decades of incipient motion studies, with special reference to gravel-bedded rivers, Water Resour. Res., 33, 1993–2029, 1997.

Bracken, L. J., Turnbull, L., Wainwright, J., and Bogaart, P.: Sediment connectivity: a framework for understanding sediment transfer at multiple scales, Earth Surf. Proc. Land., 40, 177–188, doi:10.1002/esp.3635, 2015.

Brardinoni, F. and Hassan, M. A.: Glacial erosion, evolution of river long-profiles, and the organization of process domains in mountain drainage basins of coastal British Columbia, J. Geophys. Res., 111, F01013, doi:10.1029/2005JF000358, 2006.

Brardinoni, F. and Hassan, M. A.: Glacially-induced organisation of channel-reach morphology in mountain streams, J. Geophys. Res., 112, F03013, doi:10.1029/2006JF000741, 2007.

Brardinoni, F., Hassan, M. A., Rollerson, T., and Maynard, D.: Colluvial sediment dynamics in mountain drainage basins, Earth Planet. Sc. Lett., 284, 310–319, 2009.

Brardinoni, F., Church, M., Simoni, A., and Macconi, P.: Lithologic and glacially-conditioned controls on debris-flow sediment dynamics, Geology, 40, 455–458, 2012.

ESURFD
3, 417–458, 2015

Brummer, C. J. and Montgomery, D. R.: Downstream coarsening in headwater channels, Water Resour. Res., 39, 1294, doi:10.1029/2003WR001981, 2003.

Bunte, K. and Abt, S. R.: Sampling surface and subsurface particle-size distributions in wadable gravel-and cobble-bed streams for analyses in sediment transport, hydraulics, and streambed monitoring, Gen. Tech. Rep. RMRS-GTR-74, U. S. Department of Agriculture, Forest Service, Rocky Mountain Research Station, Fort Collins, CO, 428 pp., 2001.

Camenen, B., Le Coz, J., Paquier, A., and Lagouy, M.: An estimation of gravel mobility over an alpine river gravel bar (Arc en Maurienne, France) using PIT-tag tracers, in: 5th International Conference on Fluvial Hydraulics (River Flow 2010), 8–10 September 2010, Braunschweig, Germany, 953–960, 2010.

Cavalli, M., Trevisani, S., Comiti, F., and Marchi, L.: Geomorphometric assessment of spatial sediment connectivity in small Alpine catchments, Geomorphology, 188, 31–41, 2013.

Church, M. and Hassan, M. A.: Size and distance of travel of unconstrained clasts on a streambed, Water Resour. Res., 28, 299–303, 1992.

Comiti, F. and Mao, L.: Recent advances in the dynamics of steep channels, in: Gravel-Bed Rivers: Processes, Tools, Environments, Chichester, John Wiley & Sons , 351–377, 2012.

Comiti, F., Marchi, L., Macconi, P., Arattano, M., Bertoldi, G., Borga, M., Brardinoni, F., Cavalli, M., D'Agostino, V., Penna, D., and Theule, J.: A new monitoring station for debris flows in the European Alps: first observations in the Gadria basin, Nat. Hazards, 73, 1175–1198, 2014.

D'Agostino, V. and Lenzi, M. A.: Bedload transport in the instrumented catchment of the Rio Cordon: Part II: Analysis of the bedload rate, Catena, 36, 191–204, 1999.

Ergenzinger, P. J. and Custer, S. G.: Determination of bedload transport using naturally magnetic tracers: first experiences at Squaw Creek, Gallatin County, Montana, Water Resour. Res., 19, 187–193, 1983.

Gilbert, G. K. and Murphy, E. C.: The transportation of debris by running water, Vol. 86, US Government Printing Office, Washington, 1914.

Gomez, B. and Church, M.: An assessment of bed load sediment transport formulae for gravel bed rivers, Water Resour. Res., 25, 1161–1186, 1989.

Green, K.G, Alila, Y., and Brardinoni, F.: Patterns of bedload entrainment and transport in forested headwater streams of the Columbia Mountains, Canada, Earth Surf. Proc. Land., 40, 427–446, doi:10.1002/esp.3642, 2015.

ESURFD
3, 417–458, 2015

Habersack, H. M. and Laronne, J. B.: Evaluation and improvement of bed load discharge formulas based on Helley-Smith sampling in an alpine gravel bed river, J. Hydraul. Eng., 128, 484–499, 2002.
Habler, G., Thöni, M., and Grasemann, B.: Cretaceous metamorphism in the Austroalpine Matsch Unit (Eastern Alps): the interrelation between deformation and chemical equilibration processes, Miner. Petrol., 97, 149–171, 2009.
Halwas, K. L. and Church, M.: Channel units in small, high gradient streams on Vancouver Island, British Columbia, Geomorphology, 43, 243–256, 2002.
Haschenburger, J. K. and Church, M.: Bed material transport estimated from the virtual velocity of sediment, Earth Surf. Proc. Land., 23, 791–808, 1998.
Hassan, M. A. and Ergenzinger, P.: Use of tracers in fluvial geomorphology, in: Tools in Fluvial Geomorphology, Chichester, John Wiley & Sons, 397–423, 2003.
Hassan, M. A., Church, M., and Schick, A. P.: Distance of movement of coarse particles in gravel bed streams, Water Resour. Res., 27, 503–511, 1991.
Hassan, M. A., Church, M., and Ashworth, P. J.: Virtual rate and mean distance of travel of individual clasts in gravel-bed channels, Earth Surf. Proc. Land., 17, 617–627, 1992.
Hassan, M. A., Voepel, H., Schumer, R., Parker, G., and Fraccarollo, L.: Displacement characteristics of coarse fluvial bed sediment, J. Geophys. Res.-Earth, 118, 155–165, 2013.
Hoffmann, T., Muller, T., Johnson, E. A., and Martin, Y. E.: Postglacial adjustment of steep, low-order drainage basins, Canadian Rocky Mountains, J. Geophys. Res.-Earth, 118, 2568–2584, 2013.
Houbrechts, G., Van Campenhout, J., Levecq, Y., Hallot, E., Peeters, A., and Petit, F.: Comparison of methods for quantifying active layer dynamics and bedload discharge in armoured gravel-bed rivers, Earth Surf. Proc. Land., 37, 1501–1517, doi:10.1002/esp.3258, 2012.
Hungr, O.: Classification and terminology, in: Debris-Flow Hazards and Related Phenomena, edited by: Jakob, M. and Hungr, O., Springer, Berlin, 9–23, 2005.
Johnston, P., Bérubé, F., and Bergeron, N. E.: Development of a flatbed passive integrated transponder antenna grid for continuous monitoring of fishes in natural streams, J. Fish Biol., 74, 1651–1661, 2009.
Lamarre, H. and Roy, A. G.: A field experiment on the development of sedimentary structures in a gravel-bed river, Earth Surf. Proc. Land., 33, 1064–1081, 2008.
Lamarre, H., MacVicar, B., and Roy, A. G.: Using passive integrated transponder (PIT) tags to investigate sediment transport in gravel-bed rivers, J. Sediment. Res., 75, 736–741, 2005.

ESURFD
3, 417–458, 2015

Laronne, J. B. and Carson, M. A.: Interrelationships between bed morphology and bed-material transport for a small, gravel-bed channel, Sedimentology, 23, 67–85, 1976.
Lenzi, M. A.: Displacement and transport of marked pebbles, cobbles and boulders during floods in a steep mountain stream, Hydrol. Process., 18, 1899–1914, 2004.
Leopold, L. B., Emmett, W. W., and Myrick, R. M. (Eds.): Channel and Hillslope Processes in a Semiarid Area, New Mexico, US Government Printing Office, Washington, 1966.
Liébault, F. and Laronne, J. B.: Evaluation of bedload yield in gravel-bed rivers using scour chains and painted tracers: the case of the Esconavette Torrent (southern French Prealps), Geodin. Acta, 21, 23–34, 2008.
Liébault, F., Bellot, H., Chapuis, M., Klotz, S., and Deschâtres, M.: Bedload tracing in a high-sediment-load mountain stream, Earth Surf. Proc. Land., 37, 385–399, 2012.
Mao, L. and Lenzi, M. A.: Sediment mobility and bedload transport conditions in an alpine stream, Hydrol. Process., 21, 1882–1891, 2007.
Martin, Y.: Evaluation of bed load transport formulae using field evidence from the Vedder River, British Columbia, Geomorphology, 53, 75–95, 2003.
Montgomery, D. R. and Buffington, J. M.: Channel reach morphology in mountain drainage basins, Geol. Soc. Am. Bull., 109, 596–611, 1997.
Nakato, T.: Tests of selected sediment-transport formulas, J. Hydraul. Eng., 116, 362–379, 1990.
Nichols, M. H.: A radio frequency identification system for monitoring coarse sediment particle displacement, Appl. Eng. Agric., 20, 783–787, 2004.
Nitsche, M., Rickenmann, D., Turowski, J. M., Badoux, A., and Kirchner, J. W.: Evaluation of bedload transport predictions using flow resistance equations to account for macro-roughness in steep mountain streams, Water Resour. Res., 47, W08513, doi:10.1029/2011WR010645, 2011, 2011.
Parker, G., Klingeman, P. C., and McLean, D. G.: Bedload and size distribution in paved gravel-bed streams, J. Hydr. Eng. Div.-ASCE, 108, 544–571, 1982.
Rickenmann, D.: Comparison of bed load transport in torrents and gravel bed streams, Water Resour. Res., 37, 3295–3305, 2001.
Schmidt, K. H. and Ergenzinger, P.: Bedload entrainment, travel lengths, step lengths, rest periods – studied with passive (iron, magnetic) and active (radio) tracer techniques, Earth Surf. Proc. Land., 17, 147–165, 1992.

ESURFD
3, 417–458, 2015

Schneider, J., Hegglin, R., Meier, S., Turowski, J. M., Nitsche, M., and Rickenmann, D.: Studying sediment transport in mountain rivers by mobile and stationary RFID antennas, in: River Flow, Braunschweig, Germany, Bundesanstalt für Wasserbau (BAW), Vol. 2010, 1723–1730, 2010.

Schneider, J. M., Turowski, J. M., Rickenmann, D., Hegglin, R., Arrigo, S., Mao, L., and Kirchner, J. M.: Scaling relationships between bed load volumes, transport distances, and stream power in steep mountain channels, J. Geophys. Res.-Earth, 119, 533–549, 2014.

Sear, D. A., Damon, W., Booker, D. J., and Anderson, D. G.: A load cell based continuous recording bedload trap, Earth Surf. Proc. Land., 25, 659–672, 2000.

Takayama, S.: Bedload movement in torrential mountain streams, Tokyo Geography Papers, 9, 169–188, 1965.

Weekes, A. A., Torgersen, C. E., Montgomery, D. R., Woodward, A., and Bolton, S. M.: A process-based hierarchical framework for monitoring glaciated alpine headwaters, Environ. Manage., 50, 982–997, 2012.

Wohl, E.: Mountain Rivers Revisited, American Geophysical Union Monograph, Washington DC, Vol. 19, 573 pp., 2010.

ESURFD
3, 417–458, 2015

Table 1. Summary information on the tracer clasts released at Upper Strimm and Lower Strimm.

Site	Release date	*N*	*B* axis (mm) Min	*B* axis (mm) Max	Weight (g) Min	Weight (g) Max	Rib spacing (m)
US	31 Aug 2011	80	23	155	89	1129	5
	28 Sep 2011	79	37	102	117	1482	5
	14 Jun 2012	100	34	108	92	1432	5
LS	25 Jul 2011	101	35	229	83	6525	3
	29 Aug 2011	69	43	160	177	3085	3
	7 Jul 2013	61	49	132	179	2328	3

ESURFD
3, 417–458, 2015

Table 2. Weight categories (g) of the tracer clasts.

W1	W2	W3	W4	W5	W6	W7	W8
< 200	201–400	401–600	601–800	801–1000	1001–1500	1501–3000	> 3000

ESURFD
3, 417–458, 2015

Table 3. Estimates of sediment volumes (m^3) transported at Upper Strimm.

Survey	28 Sep 2011	14 Jun 2012	3 Jul 2012	11 Sep 2012	4 Oct 2012	27 Jun 2013	1 Oct 2013	13 Jun 2014
Q_{max} ($m^3\ s^{-1}$)	0.36	0.66	0.55	0.33	0.32	1.13	0.72	0.95
V (m^3)	0.206	0.256	0.224	0.362	0.111	1.096	0.488	1.060

ESURFD
3, 417–458, 2015

Table 4. Estimates of sediment volumes (m^3) transported at Lower Strimm.

Survey	27 Sep 2011	18 May 2012	28 Jun 2012	21 Aug 2012	25 Oct 2012	21 May 2013	2 Jul 2013	2 Oct 2013	16 Jul 2014
Q_{max} ($m^3 s^{-1}$)	0.58	0.53	1.05	0.65	0.51	0.38	1.81	1.01	1.51
V (m^3)	3.533	3.104	121.965	2.396	8.742	0.996	334.614	24.828	89.520

ESURFD
3, 417–458, 2015

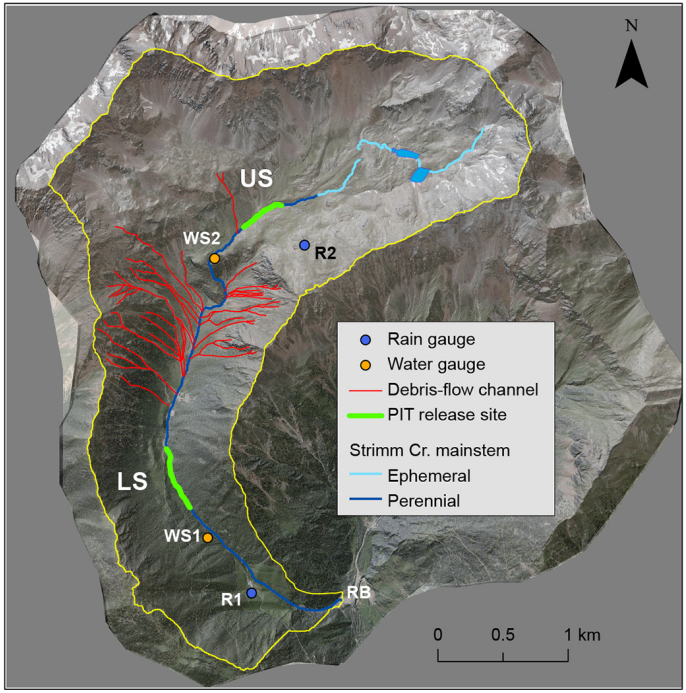

Figure 1. Map of the Strimm Creek basin showing the location of the tracers' release sites in Upper Strimm (US) and Lower Strimm (LS) along the channel main stem. Hydrologic classification was delineated during summer field surveys. Debris flow-dominated tributaries (red artwork) are mapped from historical aerial photo interpretation and fieldwork. WS1 = water stage gauging in Lower Strimm; WS2 = water stage gauging in Upper Strimm; R1 = rain gauge station at Strimmhof; R2 = rain gauge station in Upper Strimm; RB = retention basin at Strimm Creek outlet.

ESURFD
3, 417–458, 2015

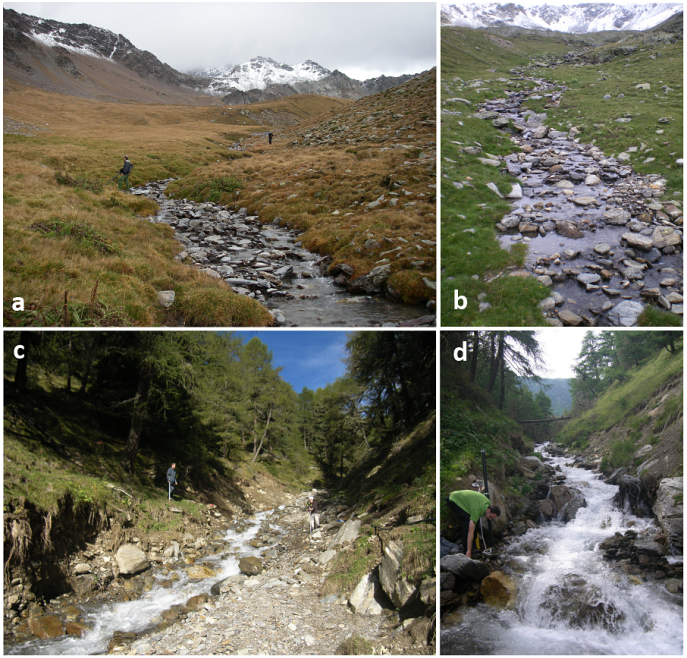

Figure 2. (a) Upper Strimm flowing across the hanging valley floor in decoupled conditions; and **(b)** detail of rapids channel-reach morphology (i.e., transverse ribs on a shallow bed) at low flow conditions. **(c)** Lower Strimm in strongly coupled conditions characterized by step-pool and boulder-cascade morphology at low flow conditions with banks eroded by the 2010 debris flow; and **(d)** the water gauging station (WS1) to the left of the picture.

ESURFD
3, 417–458, 2015

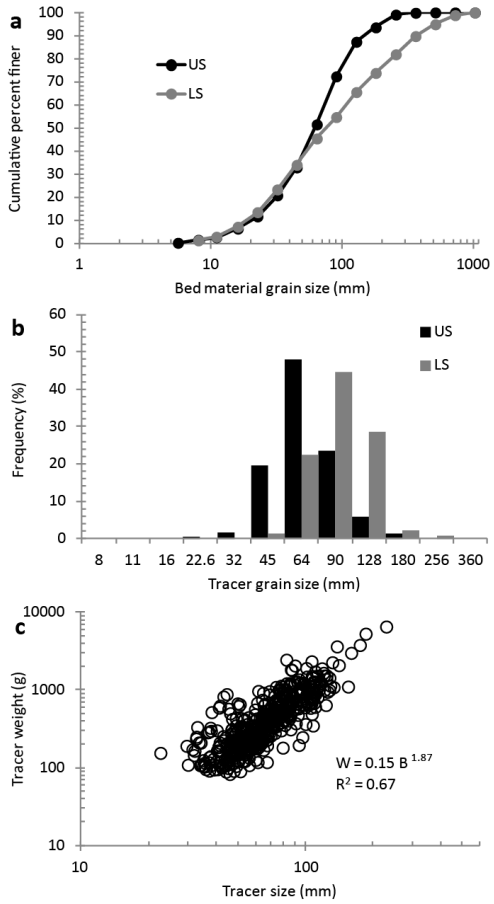

Figure 3. (a) Surface grain size distribution in US (D_{30} = 42 mm, D_{50} = 62 mm, D_{84} = 119 mm, and D_{90} = 148 mm) and LS (D_{30} = 40 mm, D_{50} = 76 mm, D_{84} = 281 mm and D_{90} = 368 mm); and **(b)** corresponding tracer size (*b* axis). **(c)** Tracer weight as a function of tracer size (*b* axis).

ESURFD
3, 417–458, 2015

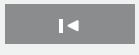

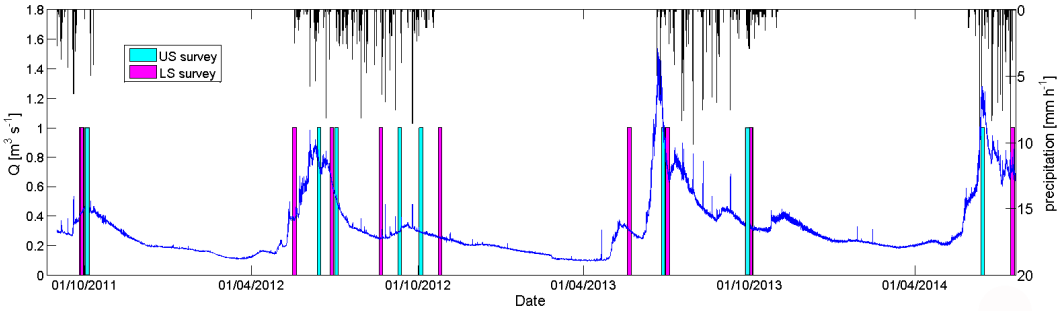

Figure 4. Water discharge hydrograph at WS2 station and the temporal distribution of tracer surveys in US (cyan bars) and LS (purple bars). Vertical black bars indicate hourly rainfall intensity recorded at the non-heated pluviometer (R2).

ESURFD
3, 417–458, 2015

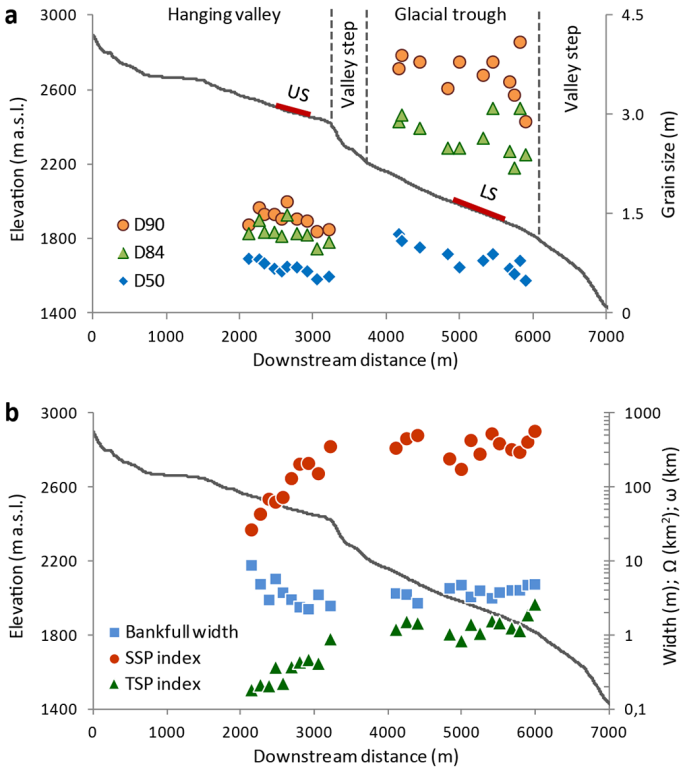

Figure 5. Longitudinal profile of Strimm Creek and the downstream variation of: **(a)** D_{50}, D_{84}, and D_{90}; and **(b)** bankfull channel width and indices of total (Ω) and specific (ω) stream power. US and LS mark the locations of tracers' release.

ESURFD
3, 417–458, 2015

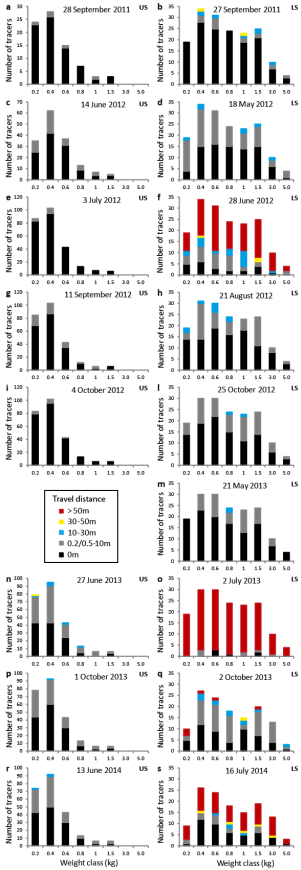

Figure 6. Stacked bar graphs showing the inter-survey frequency distributions of tracer travel distances across weight categories. Travel distances are stratified into five classes including: no motion, < 10, 10–30, 30–50, and > 50 m. Note disparity in travel distances between US (left hand side panels) and LS (right hand side panels).

ESURFD
3, 417–458, 2015

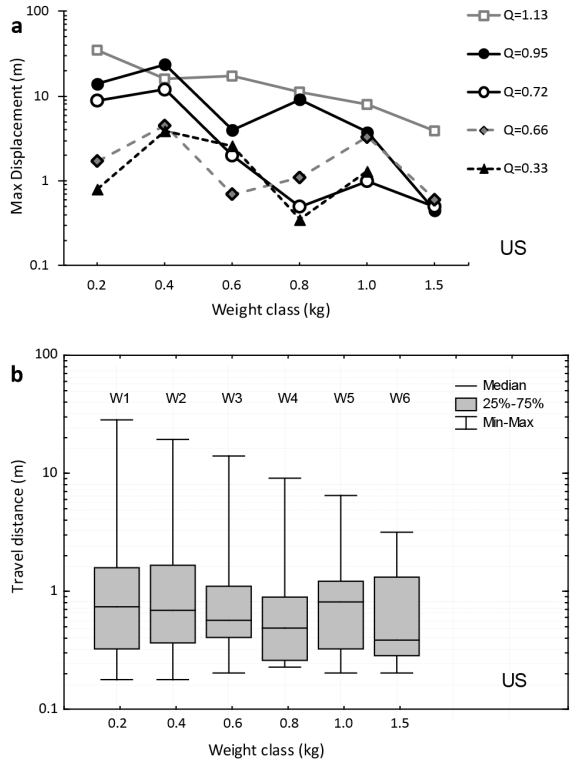

Figure 7. (a) Tracer maximum travel distance as a function of weight and stratified by inter-survey peak discharge (Q_{max}) in Upper Strimm (US). **(b)** Boxplot showing the distribution of tracer travel distances across weight classes in Upper Strimm (US).

ESURFD
3, 417–458, 2015

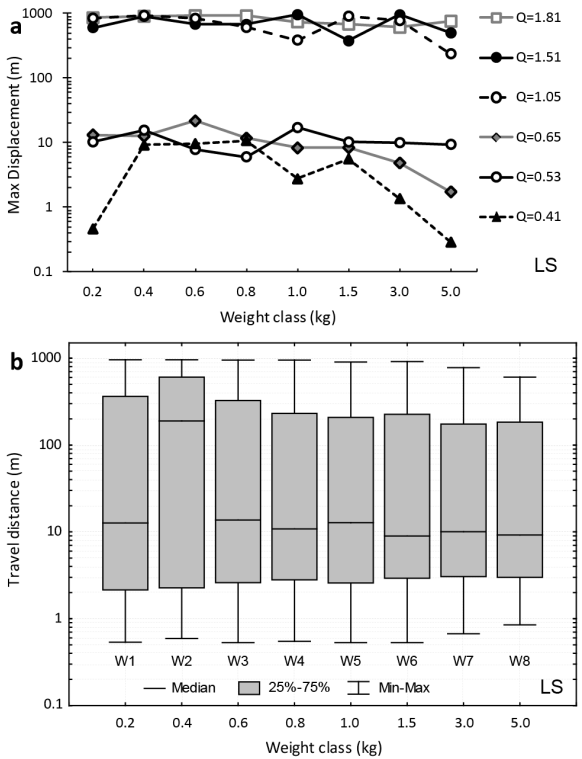

Figure 8. (a) Tracer maximum travel distance as a function of weight and stratified by inter-survey peak discharge (Q_{max}) in Lower Strimm (LS). **(b)** Boxplot showing the distribution of tracer travel distances across weight classes in Lower Strimm (LS).

ESURFD
3, 417–458, 2015

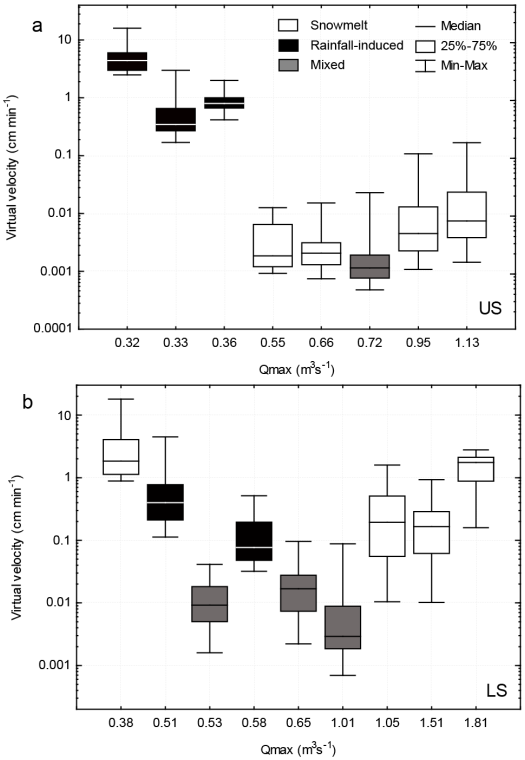

Figure 9. Boxplots of the tracers' virtual velocities in relation to the corresponding intra-survey peak discharge (Q_{max}) in: **(a)** Upper Strimm (US); and **(b)** Lower Strimm (LS). The flow regime of intra-survey periods is classified in snowmelt, rainfall-induced, and mixed (a combination of the two).

ESURFD
3, 417–458, 2015

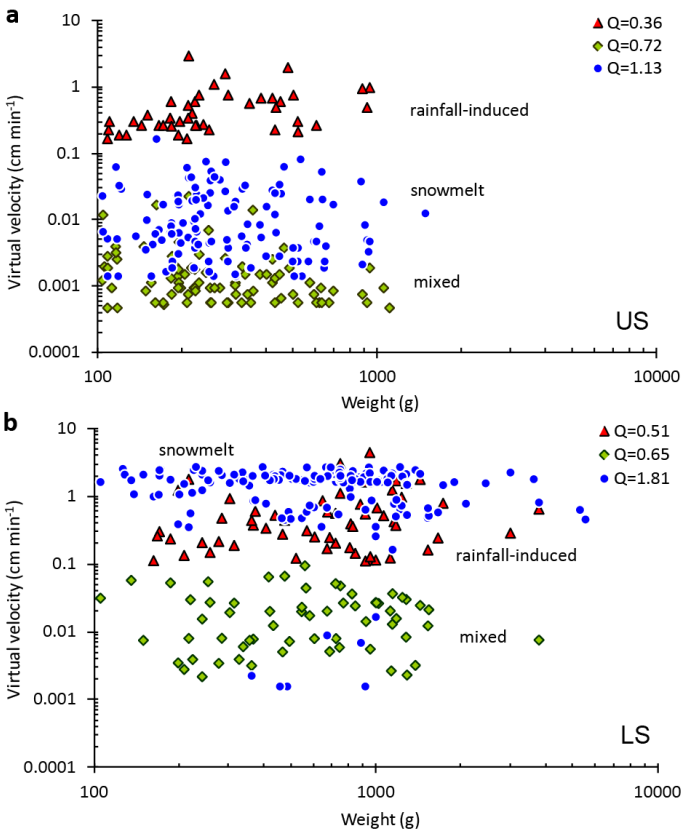

Figure 10. Tracers' virtual velocities as a function of weight for three selected peak discharges in Upper Strimm **(a)** and in Lower Strimm **(b)**. The selected peak discharges for US and LS correspond to the same inter-survey periods and therefore are directly comparable. Red triangles refer to rainfall-induced velocities (i.e., summer–fall 2012), blue circles to snowmelt-related velocities (i.e., spring–summer 2013), and green diamonds are associated with mixed snowmelt-rainfall periods.

ESURFD
3, 417–458, 2015

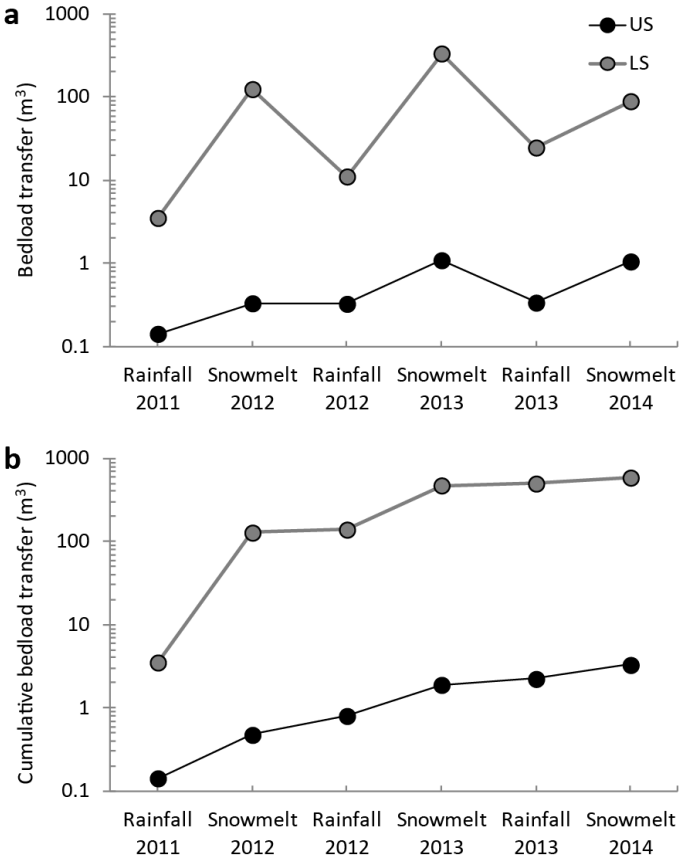

Figure 11. Non-cumulative **(a)** and cumulative **(b)** seasonal representation of estimated bedload volumes transported in Upper Strimm (US) and Lower Strimm (LS). Note the efficiency of snomelt transport periods and the nearly two-order magnitude difference between US and LS.

ESURFD
3, 417–458, 2015

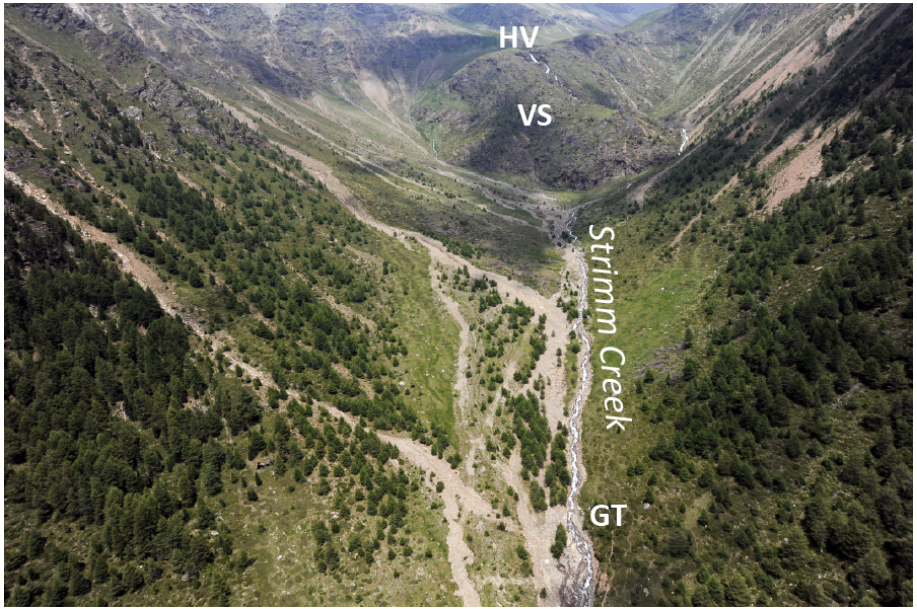

Figure 12. Oblique aerial view of the mid Strimm Creek basin taken after the storm event of 12 July 2010. Note the lateral colluvial channels activated during the event that have delivered material directly to Strimm Creek, activating a debris flow, which downstream transformed into a debris flood, and that deposited about 15 000 m^3 of debris in the retention basin located at the basin outlet. In the background are visible the hanging valley (HV) and the rocky valley step (VS) that joins abruptly with the U-shaped relict glacial trough (GT).

ESURFD
3, 417–458, 2015